International Journal of Civil Engineering

Water-Hydraulic Structure

Technical Note

Temperature stress and surface insulation measures of concrete face slabs during cold wave period

L. Yanlong[1,*], L. Shouyi[1], Y. Yang[1], T. Xing[1]

Received: September 2013, Revised: September 2014, Accepted: December 2014

Abstract

This study simulates the temperature field and temperature stress of concrete face slabs, considering the cold waves that occur during construction as well as the contact friction between the face slabs and the cushion layer. The results show that when a cold wave occurs during construction, the surface and center temperature of the face slabs continually drop with the outside air temperature, with the surface temperature drop being the largest. In addition, the surface and center of face slabs are subjected to tensile stress, with the maximum principal stress on the surface being greater than that on the center. The maximum principal stress of the surface and center occurs at approximately half of the dam height. This study also examines the surface insulation of concrete face slabs. Surface insulation can significantly improve the temperature drop range and the maximum principal stress amplitude caused by the cold wave. A stronger heat preservation results in smaller tensile stress and an increase in the amplitude of face slabs.

Keywords: *Concrete face rockfill dam, Cold wave, Temperature stress, Surface insulation, Contact friction.*

1. Introduction

Hydropower development in China is entering a rapid development period, the construction of ultra-high (300 m level) concrete faced rockfill dam become an inevitable trend, such as the planed Dashixia dam on the Kumalake river in Xinjiang province, Cihaxia hydropower station on Yellow River in Qinghai province and so on(Yang et al., 2012; Ma, 2007). All of these dams are in cold area in western China, the adverse climate conditions and large temperature difference between day and night poses challenges to the construction of the concrete slabs. The concrete face slab is supported by rockfill, being a long piece of thin plate, is strongly influenced by environmental temperature, particularly if a cold wave occurs during construction. In such conditions, the hydration heat temperature of the concrete inside the face slab is higher but its strength is lower. Temperature stress may cause surface cracks and penetrating cracks in the face slabs (Li et al., 2010). Thus, under the condition that a cold wave occurs during construction, the change and distribution law of temperature field and temperature stress are examined in this study. Heat preservation, which is a significant factor guiding damming technology development of concrete face rockfill dams, is also measured.

** Corresponding author: liyanlong@xaut.edu.cn*
1 State Key Laboratory of Eco-hydraulic Engineering in Shaanxi, Xi'an University of Technology, Xi'an, 710048, China

The temperature stress of face slabs is determined by two factors: the stress caused by temperature change and the contact constraints of the cushion layer. Temperature stress is calculated mainly through analytical calculation and the finite element method (FEM). FEM can consider changes in parameters over time, such as the temperature rise of concrete hydration, creep, elastic modulus, autogenous volume deformation, and so on, thereby making the calculation results more accurate and reliable.

Many scholars have conducted research in this area and have achieved many valuable results (Chen et al., 2011; Kim et al., 2011; Noorzaei et al., 2010; Trapko and Trapko, 2012). Hyunwook Kim and William G. Buttlar (Kim and Buttlar, 2009) investigated the low-temperature fracture behavior of concrete based on the cohesive fracture model. The triaxial strength and failure criterion of high-strength and high-performance concrete under high temperatures were discussed by Zhen-jun He and Yu-pu Song (He and Song, 2010). S. Dal Pont et al. (Pont et al., 2007) presented a coupled thermo-hydro-mechanical model to describe concrete at high temperatures. M.S. Jaafar et al. (Jaafar et al., 2007) developed a finite element computer code for the determination of temperatures within the roller-compacted concrete dam body. The physical and mechanical properties of plain concrete at elevated temperatures were examined by Omer Arioz (Arioz, 2007). M. Petkovski (Petkovski, 2010) investigated the effects of different heat-load regimes on the stress-strain behavior of partially sealed concrete under multiaxial compression. The general stress-strain

[DOI: 10.22068/IJCE.13.4.501]

relationship of concrete at elevated temperatures was discussed by M.A. Youssef and M. Moftah (Youssef and Moftah, 2007). Using DIANA software, Shuang Liu and Chao Lv (Liu and Lv, 2011) investigated the stress performance of reinforced concrete at ultra-low temperatures. Jean-Christophe Mindeguia et al. (Mindeguia et al., 2010) combined experimental and numerical simulation to investigate the spalling risk of concrete under different conditions.

To simulate the contact constraints between the face slabs and the cushion layer, traditional stress calculation methods first process the contact area as the elastic constraint so that temperature stress can be calculated. Ga Zhang and Jian-Min Zhang (Zhang and Zhang, 2009) used an elasto-plasticity damage interface element to describe the separation and re-contact between the face slab and the cushion layer at the interface. A zero-thickness interface element was used by Degao Zou et al. (Zou et al., 2013) to analyze the seismic response of the Zipingpu concrete face rockfill dam (CFRD). Yalin Arici (Arici, 2011) examined the cracking behavior of the face plate of a CFRD over its life cycle during construction, impounding, long-term deformation, and earthquake loading. Alemdar Bayraktar and Murat Emre Kartal (Bayraktar and Kartal, 2010) designed a joint between the concrete slab and the rockfill as a welded contact and investigated the linear and nonlinear response of the Torul CFRD. Alemdar Bayraktar et al. (Bayraktar et al., 2011) discussed the effects of concrete slab-rockfill interface behavior on the earthquake performance of a concrete-faced rockfill dam, considering both friction contact and welded contact. Bin Xu et al. (Xu et al., 2012) used a generalized plasticity model to simulate the construction of the Zipingpu CFRD, with zero-thickness interface elements between the face slabs and the cushions. Bingyin Zhang et al. (Zhang et al., 2004) investigated the time-dependent deformation and separation between the concrete face slab and the cushion layer. However, the relationship between the face slab and the cushion layer was processed as an "elastic restraint," and the constraint effect of the cushion layer was exaggerated. Therefore, the calculation results were insufficiently accurate.

This paper systematically analyzes the contact friction characteristics of the interface between the face slabs and the cushion layer and then establishes a contact friction element calculation model for the temperature field and temperature stress. According to the three possible contact states (fixed, sliding, and free), the model analyzes the influence of the contact friction characteristic of the contact surface on temperature field and temperature stress. A simulation analysis of the temperature field and temperature stress of the face slabs is conducted using this model. This study also measures the surface heat preservation of the concrete face slabs during construction.

2. Contact Element Calculation Model

2.1. Calculation model for temperature fields

If the contact between face slabs and the cushion layer is regarded as the contact of a point and a surface, then the heat transfer matrix of the contact friction unit can be represented as

$$[K_c]^e = \begin{cases} \dfrac{1}{R_c}\{N\}^e.\{N\}^{eT} & \text{fixed or sliding} \\ [0] & \text{free} \end{cases} \tag{1}$$

Where R_c is the thermal contact resistance of the contact friction element, which can be determined through tests, and $\{N\}^e$ is the contact friction element shape function array.

The heat load vector of the nodes can be represented as

$$\{F_c\}^e = q^e\{N\}^e \tag{2}$$

Where q^e is the heat flow from the face slab unit surface to the cushion layer contact node.

2.2. Calculation Model for Temperature Stress

Considering the temperature effect, the equivalent element stiffness of the contact friction element–constraint equations can be expressed as

$$\begin{Bmatrix} 0 & (SC')^T \\ SC' & R^T SR \end{Bmatrix}\begin{Bmatrix} \Delta\alpha \\ \Delta\sigma \end{Bmatrix} = \begin{Bmatrix} \Delta F \\ 0 \end{Bmatrix} + \begin{Bmatrix} F_T^e - (SC'')^T\Delta\sigma \\ Sa^* - (I - R^T)SR\Delta\sigma \end{Bmatrix} \tag{3}$$

The equivalent stiffness of the contact friction element–constraint matrix K_c and equivalent load vectors $f_{cT,}$ are

$$K_c = \begin{Bmatrix} 0 & (SC')^T \\ SC' & R^T SR \end{Bmatrix} \tag{4}$$

$$f_{cT} = \begin{Bmatrix} F_T^e - (SC'')^T\Delta\sigma \\ S\alpha^* - (I - R^T)SR\Delta\sigma \end{Bmatrix} \tag{5}$$

Where Δa and ΔF are the incremental nodal displacement and incremental equivalent nodal force vectors in the integral coordinate system, respectively; $\Delta\sigma$ is the incremental node contact stress vector in the local coordinate system; a^* is the constraint load vector; C' and C'' are the coordinate transformation matrices; S and R comprise the reduced matrix; F_T^{ew} is the equivalent node load produced by the strain $\{\varepsilon_T^0\}$, which is in turn caused by variable temperature T; and $\{\varepsilon_T^0\}$ and F_T^{ew} are

$$\{\varepsilon_T^0\} = [\varepsilon_{Tx}^0, \varepsilon_{Ty}^0, \gamma_{Txy}^0]^T = \alpha(1+\mu)T[1,1,0]^T \tag{6}$$

$$F_T^e = \iint_e [B]^T[D]\{\varepsilon_T^0\}dxdy \tag{7}$$

Where α is the thermal expansion coefficient; $[B]$ is element strain matrix; and $[D]$ is the element elastic matrix, respectively.

[DOI: 10.22068/IJCE.13.4.501]

According to the standard finite element integration rules, the constraint matrix K_c and the equivalent load vector f_{cT} of Types (4) and (5) can superpose to the total stiffness matrix and the total load vector in the overall temperature stress calculation.

In the actual calculation, for each time step t_i, the unit is assumed to be in a contact state (fixed, sliding, or free), to determine the corresponding constraint load vector a^*. According to Type (3), the incremental node contact stress and contact displacement are used to perform tentative calculations. If the results are consistent with the original assumption state, the calculation ends (Wang et al., 2006). Otherwise, the trial solution can be taken as the new assumption, and a new iteration is performed until convergence. When the contact state is determine, the allowable stress [σ] of the normal direction becomes the maximum tensile stress, and the allowable stress [τ] of the tangential direction is determined using the Mohr-Coulomb criterion (Lei et al., 1994).

In China, during the design of the concrete face rockfill dam, the beam on elastic foundation method is always used to calculate the temperature stress of the face slab, this method assumes that the face slab under the condition of temperature deformation, stress of the whole cross section is uniform and the face slab is treated as a elastic concrete beam which fixed on the basis of cushion, then a formula of the maximum temperature stress is derivation and established to calculate the stress along the face slab slope. This paper establishes a calculation model of contact element between the face slab and cushion layer, it improved the traditional "beam on elastic foundation method", and can simulate the contact friction characteristics between concrete face slab and cushion layer, obtain more accurate temperature stress distribution of concrete face slab.

3. Analysis of Engineering Example

3.1. Engineering Situation

The maximum dam height of the Gongboxia CFRD is 139 m, the length of the dam crest is 429 m, and the width of the dam crest is 10 m. The slope ratio of the upstream dam slope is 1:1.4, the downstream partial dam slope is 1:1.5 to 1.4, and the general dam slope is 1:1.81. The top end of the reinforced concrete face slab is 0.3 m thick, and the maximum calculation thickness at the base is 0.76 m. The vertical seams of the face slab are set according to the stress-deformation calculation results of the dam body. The gap of the vertical seams in the tensile zone is 6 m, whereas the gap of vertical seams in the compressive zone is 12 m. Seams are not set along the altitude direction. Thus, the concrete face slab of the dam is divided into 38 blocks. The length of the seam-dividing line is approximately 5,000 m, with the length of a maximum single block being approximately 219 m. The mark of the concrete face slab is C25. The face slab is reinforced by a layer of bi-directional reinforcing steel bar. According to the progress arrangement of construction, the time interval of pouring the face slab concrete was set from April 1, 2004 to June 30, 2004. Water storage in the reservoir began in mid-August 2004, and power generation started in early September 2004. The construction methods for the sub-order jump silo and single-block sliding form placement can be used in the construction time section of the face slab concrete. The sliding lifting speed of the sliding form is 1.5 m per hour on average. The standard profile of the dam is shown in Fig. 1.

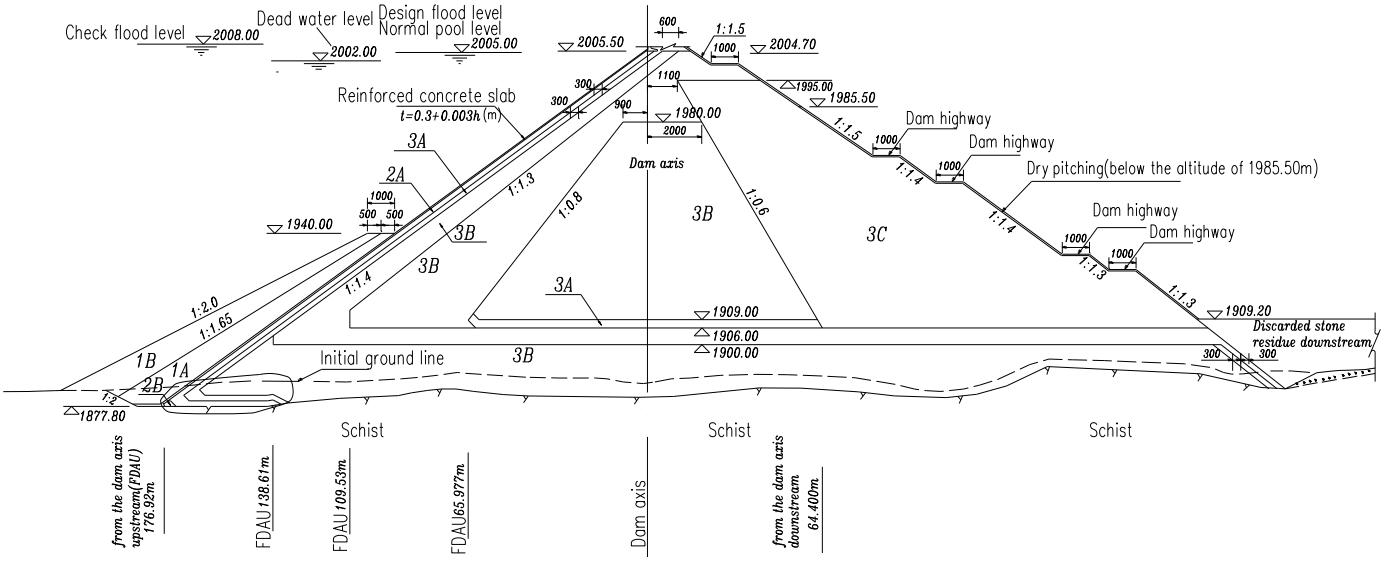

Fig. 1 Standard Profile of Dam

[DOI: 10.22068/IJCE.13.4.501]

3.2. Finite element model

Given that each face slab is poured single-handedly in succession and the gap of pouring conjoint blocks is approximately 14 d, the mutual influence of temperature fields between the conjoint blocks of the face slab is extremely weak and can thus be disregarded. Meanwhile, the face slab is slotted along the direction of the dam axis with a plane stress state, thus weakening the mutual influence of temperature stress between the conjoint blocks of the face. Therefore, this study selects the dam section including face slab F9 as the research object. The construction period of F9 was from April 5, 2004 to August 10, 2004; the dam began storing water on August 11, 2004. The highest water storage level is the normal high water level at 2,005 m. The dam section integral calculation model is shown in Fig. 2. This model subdivides the calculation model into eight nodes and the hexahedron isoparametric element, including 25,040 units and 29,095 nodes.

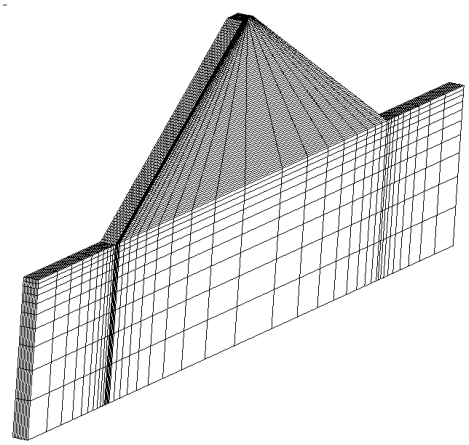

Fig. 2 Dam Section Integral Calculation Model

3.3. Parameters

Meteorological data, such as air temperature, water temperature, earth temperature, and cold wave at the Gongboxia dam-site zone, are collected from the weather station in Xunhua County, which is located in the downstream dam-site. The average duration of cold waves in recent years and the maximum temperature drop in Gongboxia are listed in Table 1 (Appendix A).

Table 1 shows that cold waves occur every month of the year at the Gongboxia dam site. May is the month with the most number of cold waves. December is the month with the least cold waves. The maximum temperature drop during cold waves occurs in May, with a maximum temperature drop of 14.2 ℃.

The elastic modulus of the concrete face slab and toe slab can be computed and can be expressed as

$$E(\tau) = 25 \times (\tau / (6.64 + \tau)) \tag{8}$$

Moreover, the thermal insulation temperature rise of concrete is expressed as

$$\theta = 42.72\tau / (2.04 + \tau) \tag{9}$$

Where τ is the age of concrete, (d).

The thermodynamic parameters of the materials of dam body and bed rock are shown in Table 2 (Appendix A).

Table 1 Average Durations of Cold Waves in Recent Years and Maximum Ranges of Temperature Drop in Gongboxia

Month	1	2	3	4	5	6	7	8	9	10	11	12	12-month total
Average time of cold wave in every year	0.7	0.9	1.4	2.4	2.6	0.8	0.7	0.9	1.0	1.4	0.5	0.3	13.6
Maximum temperature drop during cold waves (°C)	9.1	12.1	9.1	11.5	14.2	9.9	9.2	11.5	9.5	11.5	12.2	7.2	14.2

Table 2 Thermodynamic Parameters of the Materials of the Dam Body and Bed Rock

Materials	Density/	Mean specific heat/	Thermal diffusivity/	Coefficient of thermal conduction/	Heat evolution coefficient of surface/	Coefficient of linear thermal expansion/	Elastic modulus/	Poisson ratio/
	($kg \cdot m^{-3}$)	($kJ \cdot kg^{-1} \cdot ℃^{-1}$)	($m^2 \cdot h^{-1}$)	($kJ \cdot m^{-1} \cdot h^{-1} \cdot ℃^{-1}$)	($kJ \cdot m^{-2} \cdot h^{-1} \cdot ℃^{-1}$)	($10^{-6} \cdot ℃^{-1}$)	(MPa)	
Concrete of face slab and toe slab	2397	0.9793	0.00376	8.83	83.72	10.05	See eq.(8)	0.17
Cushion material and transition material	2150	0.88	0.00327	6.18	41.20	5.03	182	0.30
Rock-filling material	2200	0.735	0.00273	4.42	29.47	7.04	235	0.30
bedrock	2450	1.05	0.00309	7.95	53.0	9.05	10000	0.25

[DOI: 10.22068/IJCE.13.4.501]

4. Results and Analysis

4.1. Temperature field results and analysis

According to the cold wave data (Table 1) from the dam-site of the power station, the most disadvantageous operational conditions during cold waves are as follows. Approximately 12 d after the concrete placement for the slab (i.e., early May), a cold wave occurred and lasted for 3d with a maximum temperature drop of 14.2 ℃. During the cold wave, surface insulation intensified, and the equivalent heat evolution coefficient of slab surface changed from 12.54 $kJ \cdot m^{-2} \cdot h^{-1} \cdot ℃^{-1}$ of normal air temperature to 4.49 $kJ \cdot m^{-2} \cdot h^{-1} \cdot ℃^{-1}$.

The calculation results of the temperature field of the slab during the cold wave are shown in Fig. 3 and Fig. 4.

Fig. 3 shows the variation course of the node temperature on the surface of the slab over time at different altitudes during the cold wave. The maximum temperature drop during the 3d is 14.2℃. At this air temperature, the node temperature on the surface of the slab at different altitudes fell continuously during the cold wave. As the surface insulation was measured, the range of temperature drop was still limited, with the range of the surface temperature drop on the top of the slab being fairly large and reaching 3.7 ℃. The range of surface temperature drop at the bottom of slab was rather small at 3.6 ℃.

Fig. 4 shows the variation course of the node temperature at the center of the slab over time at different altitudes during the cold wave. The temperature drop range of the nodes at the center of slab is smaller than that on the slab surface at different altitudes. The temperature drop range at the center of the top of slab is fairly large, reaching 2.4 ℃, and the temperature drop range at the center of the bottom of the slab is rather small: 1.4 ℃.

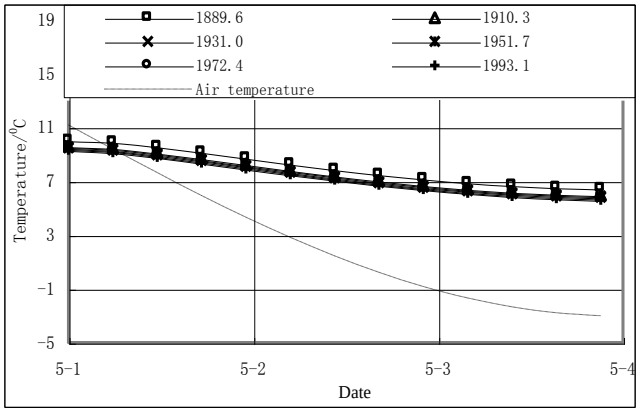

Fig. 3 Time Graph of Temperature on the Surface of the Slab During the Cold Wave

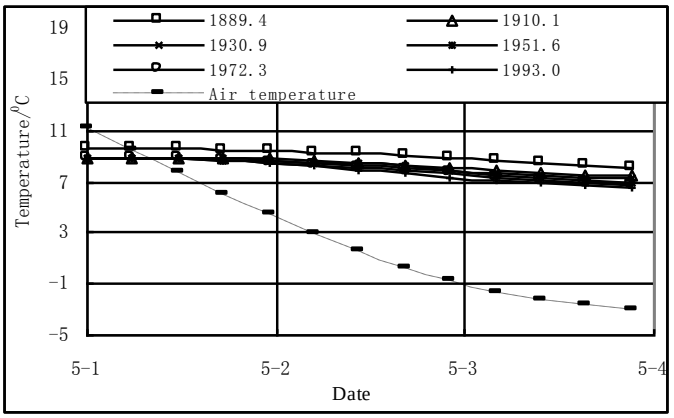

Fig. 4 Time Graph of the Temperature in the Center of the Slab During the Cold Wave

4.2. Temperature stress results and analysis

According to the above calculation s concerning the thermal field of the slab during the cold wave, considering variation over time of the elastic modulus and creep strength of the slab concrete, the node temperature is regarded as a load to calculate the corresponding thermal stress.

The calculation results of the maximum principal stress on the surface and center of the slab during the cold wave are shown in Figs. 5 and 6.

Fig. 5 shows the distribution of the maximum principal on the surface and center of the slab along different layers at the beginning of the cold wave. The cold wave occurred after the maximum temperature drop, and the temperature of the slab rose with air temperature. However, the tensile stress accumulated during the time interval of the maximum temperature drop did not disappear. Thus, tensile stress still existed on the surface and center of the slab at the beginning of the cold wave. Given that the top of the slab was free of restriction, the peripheral joints were set at the top, thus making free shrinkage deformation possible. Thus, the maximum principal stress on the slab attributed to shrinkage resulting from temperature drop occurred mid-slab, that is, at half the dam height. The maximum principal stress on the surface of slab was 0.33 MPa, and that in the center was 0.23 MPa.

Fig. 6 shows the distribution of the maximum principal stress on the surface and center of the slab along different layers at the end of the cold wave. Fig. 5 shows that the temperature drop from the cold wave causes the temperature on the surface and the center to fall, thereby increasing the tensile stress at both areas. However, the temperature drop range on the surface is larger than that in center, and the increment of the maximum principal stress on the slab surface is apparently larger than that in the center. At this moment, the maximum principal stress on the slab surface is 1.15 MPa, with the increment range being 0.82 MPa, compared with that during the beginning of the cold wave. In addition, the maximum principal stress at the slab center is 0.44 MPa, with the increment range being 0.21 MPa, compared with that during the beginning of the cold wave.

[DOI: 10.22068/IJCE.13.4.501]

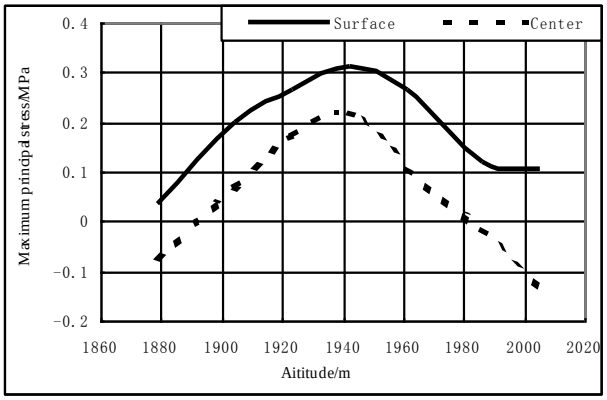

Fig. 5 Distribution Chart of Maximum Principal Stress on Surface and Center of Slab at Beginning of the Cold Wave

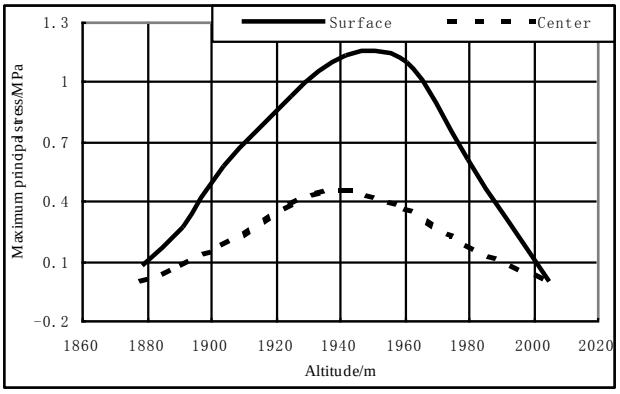

Fig. 6 Distribution Chart of Maximum Principal Stress on Surface and Center of Slab at the End of the Cold Wave

5. Face Slab Surface Insulation Measures

Considering the given operational condition of a cold wave, thermal stress is calculated in this paper at different levels of surface insulation. The comparison of the different calculations is shown in Table 3 (Appendix A).

According to the control standard of thermal stress for the foundation concrete of this power station, the sum of the thermal stress experienced by the slab concrete caused by temperature differences should not exceed 1.8 MPa. Evidently, if the slab surface is not protected immediately and effectively when a cold wave occurs and the maximum principal stress on the surface at the end of the cold wave reaches 2.35 MPa, then the likeliest outcome is that cracks would appear in the slab surface, and the stress shifts to the center of the slab. At this moment, with the principal stress on the slab center at 1.17 MPa, this will possibly make the crack stretch inward until the thickness of the whole slab is traversed, consequently forming through cracks. Table 3 compares the condition of cold wave occurrence during construction period with the condition of a bare slab surface (β = 83.72 kJ·m^{-2}·h^{-1}·℃$^{-1}$). The increment range of the maximum principal stress between the beginning and the end of the cold wave can be decreased significantly by taking surface insulation measures; the better the surface insulation measures taken, the more apparent the reduction. The reason for this outcome is that taking surface insulation measures on the surface can decrease the temperature drop range of the whole slab, particularly the slab surface. Thus, monitoring and predicting sudden air temperature drops, such as cold waves, should be done during the construction period. At the approach of a cold wave, the slab surface should be protected in time.

According to the above-mentioned thermal stress calculation results, and based on the control standard of thermal stress of concrete in the power station, the researcher suggests that at the approach of a cold wave, the degree of protection of the slab surface should be appropriate such that the coefficient of the equivalent heat evolution should meet the condition of $\beta \leq 4.49$ kJ·m^{-2}·h^{-1}·℃$^{-1}$.

Table 3 Comparison of Thermal Stress at Different Surface Protective Measures During Cold Waves

Surface protective measures	Equivalent heat evolution coefficient/ (kJ·m^{-2}·h^{-1}·℃$^{-1}$)	Surface of slabs		Center of slabs	
		Maximum principal stress after cold wave / (MPa)	Amplification of maximum principal stress during cold wave / (MPa)	Maximum principal stress after cold wave / (MPa)	Amplification of maximum principal stress during cold wave / (MPa)
No protection	83.72	2.35	1.35	1.17	0.50
Common protection	12.54	1.38	0.96	0.88	0.27
Reinforcing protection	4.49	1.15	0.82	0.44	0.21

6. Conclusions

This paper considering the cold waves that occur during the construction period of the concrete face slab as well as the contact friction characteristics between the face slab and the cushion layer, establishes a contact friction element calculation model for the temperature field and temperature stress, simulates the temperature field and temperature stress of concrete face slab. The research shows that: when cold waves occur during the construction period, the temperature on the surface and center of the slab falls continuously, with the temperature drop range of the slab surface being the largest. Considering that surface insulation measures can significantly reduce the temperature drop range, t king better surface insulation measures results in greater reduction. When cold waves occur during the construction period, the maximum principal stress on the slab surface is significantly larger than that at the center. The increment of the maximum principal stress from the beginning to the end of the cold wave can be significantly reduced by taking surface insulation measures; this reduction effect is likewise greater with better surface insulation measures. Combined with the thermal stress control standard for concrete at power stations, the researcher suggests that at the approach of a

[DOI: 10.22068/IJCE.13.4.501]

cold wave, the protection standard of the slab surface should be sufficient such that the coefficient of the equivalent heat evolution meets the condition of $\beta \leq 4.49\ kJ \cdot m^{-2} \cdot h^{-1} \cdot ℃^{-1}$.

There are many water conservancy projects under construction or planed in alpine region in western China, among them multi-seat ultra-high (200 ~ 300m level) concrete faced rockfill dam are in the majority(Ma, 2011), considering the cold waves that occur during the construction period of the concrete face slab, establishes a contact friction element calculation model to analysis the contact friction characteristics between the face slab and the cushion layer, and investigates the surface insulation measures of concrete face slab, it has practical reference to the construction of similar projects.

Acknowledgment: This research is financially supported by the National Natural Science Foundation of China (Nos. 51309190), the Doctoral Program of Higher Education of China (Nos. 20126118120015), Xi'an Science and Technology Project (CXY1349(7)), Program 2013KCT-015 for Shaanxi Provincial Innovative Research Team, Special funds for the development of characteristic key disciplines in the local university by the central financial supported(No.106-5X1205).

References

[1] Zeyan Yang, Jianping Zhou, Liqun Su, Xiaohu Du, Yongjun Sun. Review on the research of adaptability and countermeasures of 300m-level high CERD, Water Power, 2012, Vol. 38, pp. 25-29.

[2] Hongqi Ma, Keming Cao.. Key technical issues related to super-high concrete slab dam, Engineering Science, 2007, Vol. 9, pp. 4-10.

[3] Shou-yi Li, Yan-long Li, Zheng Si, Xiao-fei Zhang. A seepage computational model of face slab cracks based on equi-width joint constant flow, Advances in Engineering Software, 2010, Vol. 41, pp. 1000-1004.

[4] Chen Shoukai, Meng Meili, Liu Qiuchang, Wang Zhenhong. impact of diurnal temperature difference on the stress of thin-walled concrete structure, Journal of Hydroelectric Engineering, 2011, Vol. 37, pp. 27-30.

[5] Sunghwan Kim, Kasthurirangan Gopalakrishnan, Halil Ceylan. A simplified approach for predicting early-age concrete pavement deformation, Journal of Civil Engineering and Management, 2011, Vol. 17, pp. 27-35.

[6] Jamaloddin Noorzaei, Aeid. A. Abdulrazeg, Mohamed Saleh Jaafar, Omid Kohnehpooshi. Non–linear analysis of an integral bridge, Journal of Civil Engineering and Management, 2010, Vol. 16, pp. 387-394.

[7] Wojciech Trapko, Tomasz Trapko. Load-bearing capacity of compressed concrete elements subjected to repeated load strengthened with CFRP materials, Journal of Civil Engineering and Management, 2012, Vol. 18, pp. 590-599.

[8] Hyunwook Kim, William G. Buttlar. Finite element cohesive fracture modeling of airport pavements at low temperatures, Cold Regions Science and Technology, 2009, Vol. 57, pp. 123-130.

[9] Zhen-jun He, Yu-pu Song. Triaxial strength and failure criterion of plain high-strength and high-performance concrete before and after high temperatures, Cement and Concrete Research, 2010, Vol. 40, pp. 171–178.

[10] Dal Pont S, Durand S, Schrefler BA. A multiphase thermo-hydro-mechanical model for concrete at high temperatures - Finite element implementation and validation under LOCA load, Nuclear Engineering and Design, 2007, Vol. 237, pp. 2137-2150.

[11] Jaafar MS, Bayagoob KH, Noorzaei J, Waleed AM Thanoon. Development of finite element computer code for thermal analysis of roller compacted concrete dams, Advances in Engineering Software, 2007, Vol. 38, pp. 886-895.

[12] Omer Arioz. Effects of elevated temperatures on properties of concrete, Fire Safety Journal, 2007, Vol. 42, pp. 516-522.

[13] Petkovski M. Effects of stress during heating on strength and stiffness of concrete at elevated temperature, Cement and Concrete Research, 2010, Vol. 40, pp. 1744-1755.

[14] Youssef MA, Moftah M. General stress–strain relationship for concrete at elevated temperatures, Engineering Structures, 2007, Vol. 29, pp. 2618-2634.

[15] Shuang Liu, Chao Lv. Reinforced concrete beam stress performance at ultra-low temperature, Procedia Engineering, 2011, Vol. 24, pp. 370-374.

[16] Jean-Christophe Mindeguia, Pierre Pimienta, Albert Noumowé, Mulumba Kanema. Temperature, pore pressure and mass variation of concrete subjected to high temperature-Experimental and numerical discussion on spalling risk, Cement and Concrete Research, 2010, Vol. 40, pp. 477-487.

[17] Ga Zhang, Jian-Min Zhang. Numerical modeling of soil - structure interface of a concrete-faced rockfill dam, Computers and Geotechnics, 2009, Vol. 36, pp. 762-772.

[18] Degao Zou, Bin Xu, Xianjing Kong, Huabei Liu, Yang Zhou. Numerical simulation of the seismic response of the Zipingpu concrete face rockfill dam during the Wenchuan earthquake based on a generalized plasticity model, Computers and Geotechnics, 2013, Vol. 49, pp. 111-122.

[19] Yalin Arici. Investigation of the cracking of CFRD face plates, Computers and Geotechnics, 2011, Vol. 38, pp. 905-916.

[20] Alemdar Bayraktar, Murat Emre Kartal. Linear and nonlinear response of concrete slab on CFR dam during earthquake, Soil Dynamics and Earthquake Engineering, 2010, Vol. 30, pp. 990-1003.

[21] Alemdar Bayraktar, Murat Emre Kartal, Suleyman Adanur. The effect of concrete slab–rockfill interface behavior on the earthquake performance of a CFR dam, International Journal of Non-Linear Mechanics, 2011, Vol. 46, pp. 35-46.

[22] Bin Xu, Degao Zou, Huabei Liu. Three-dimensional simulation of the construction process of the Zipingpu concrete face rockfill dam based on a generalized plasticity model, Computers and Geotechnics, 2012, Vol. 43, pp. 143-154.

[23] Bingyin Zhang JG, Wang Ruifeng Shi. Time-dependent deformation in high concrete-faced rockfill dam and separation between concrete face slab and cushion layer, Computers and Geotechnics, 2004, Vol. 31, pp. 559-573.

[24] Wang Ruijun, LI Zhanghao, Wang Dangzai, Chen Yaolong. Research on computation model of thermal stresses of interface between slabs and cushion layer, Journal of Hydroelectric Engineering, 2006, Vol. 25, pp. 58-71.

[25] Lei Xiao-yan, G.Swoboda, Du Qing-hua. Theory and application of contact-friction interface element, Chinese Journal of Geotechnical Engineering, 1994, Vol. 16, pp. 23-32.

[26] Hongqi Ma. 300 m grade concrete faced rockfill dam adaptability and countermeasures, Engineering Science, 2011, Vol. 13, pp. 4-10.

[DOI: 10.22068/IJCE.13.4.501]